J Biomech Eng 137(11), 111003 (Sep 16, 2015) (8 pages) Paper No: BIO-15-1142; doi: 10.1115/1.4031487 History: Received April 01, 2015; Revised August 22, 2015

Hemodynamics in the left atrium and its effect on ventricular flow patterns

Vijay Vedula
Department of Mechanical Engineering,
Johns Hopkins University,
3400 N. Charles Street, Baltimore, MD 21218, USA

Richard George

Division of Cardiology,
Johns Hopkins University,
733 N. Broadway, Baltimore, MD 21205, USA

Laurent Younes

Department of Applied Mathematics and Statistics,
Johns Hopkins University,
3400 N. Charles Street, Baltimore, MD 21218, USA

Rajat Mittal
*
Department of Mechanical Engineering,
Johns Hopkins University,
3400 N. Charles Street, Baltimore, MD 21218, USA

In the present study, we investigate the hemodynamics inside left atrium and understand its impact on the development of ventricular flow patterns. We construct the heart model using dynamic computed tomographic images and perform simulations using immersed boundary method based flow solver. We show that the atrial hemodynamics is characterized by a circulatory flow generated by the left pulmonary veins and a direct stream from the right ones. The complex interaction of the vortex rings formed from each of the pulmonary veins leads to vortex breakup and annihilation, thereby producing a regularized flow at the mitral annulus. A comparison of the ventricular flow velocities between the physiological and a simplified pipe-based atrium model shows that the overall differences are limited to about 10% of the peak mitral flow velocity. The implications of this finding on the functional morphology of the left heart as well the computational and experimental modeling of ventricular hemodynamics are discussed.

*Address all correspondence for other issues to this author. Email: mittal@jhu.edu

Nomenclature

LA Left Atrium.
LPVs/RPVs Left/Right Pulmonary Veins.
MO/MV Mitral Orifice/Mitral Valve.
LV Left Ventricle.
CT Computed Tomography.
EF Ejection Fraction.
Re Reynolds number.
Wo Womersely number.
U_p Peak area-averaged velocity through the mitral annulus.
p Pressure.
$\vec{u}$ Velocity vector of fluid.

1 Introduction

The left atrium (LA) has a complex structure [1–3]; the left pulmonary veins (LPVs), connected to the left lung, are positioned lower in the atrial cavity near the mitral orifice (MO) and the right pulmonary veins (RPVs) connected to the right lung are positioned higher with respect to the LA cavity. Additionally, there is a highly distensible and trabeculated muscular sac positioned near the MO, called the left atrial

appendage (LAA) [1]. While the precise role of the LAA in the functioning of the LA is not clear, it is highly prone to clot formation in pathologies such as atrial fibrillation [4, 5].

The complexity of the LA structure is complemented by its three-fold function during a cardiac cycle [2, 3, 6]. The LA acts as a conduit passage during early ventricular filling (E-wave) when the left ventricle (LV) passively relaxes and establishes a low pressure in its cavity. The atrial filling (A-wave) follows during which it acts as a booster pump forcefully delivering the blood into LV. During ventricular systole, the LA acts as a reservoir with blood from the pulmonary veins (PVs) when the mitral valve (MV) is completely closed.

The complexity of the atrial hemodynamics has been a subject of a number of studies in the past [5, 7–10]. The flow pathways from the LPVs and RPVs differ significantly [7]. The inflow from LPVs forms a rotational loop and is associated with longer pathways towards the MO although, these veins are paradoxically located proximal to it; whereas, the inflow from RPVs is more aligned with the wall directly entering the MO [7]. Additionally, it is also conjectured that the velocity distribution in the atrial vortices might produce a better washing effect in LA and avoid intra-atrial flow stasis [7]. Given the importance of the LV functioning, the question on how the atrial flow patterns effect diastolic filling in the LV has also been brought up before. It was suggested that the asymmetric filling from the PVs generate sinuous asymmetric atrial flow pathways in the LA cavity [8], which tend to preserve the blood momentum towards the valves during the cardiac cycle [8]. It was also surmised that the vorticity introduced into the LA cavity from the PVs is transported through the mitral valve downstream into the LV [10] and indicated that lack of such a vorticity transport model would produce similar ventricular flow patterns with or without the LA [10].

The vast majority of cardiac computational models to date have been single-chamber models [11–18] which have focused either on the left or the right ventricles [19–21] while the atria are modeled in highly simplistic ways. It is usual to replace the LA with a pipe or to mimic its presence by providing suitable time-dependent inflow boundary conditions [11–16]. However, the impact of this simplification on the ventricular flow development is still unclear [21].

Our primary objective is therefore to characterize the flow and vortex topology in the LA and to examine and quantify the effect of this flow on the diastolic LV flow patterns. A secondary objective is to use the results from the above analysis to determine, for studies that are focused on LV flow dynamics, the level of fidelity needed in modeling the LA. To meet these objectives, we create a left-heart model comprising the major chambers (LA, LV and Aorta (Ao)) using dynamic 4D CT data, while the MV is modeled based on previously reported prescribed kinematics approach [22, 23] using the leaflet angles measured from the present 4D CT data. We then perform blood flow simulations by solving the incompressible Navier-Stokes equations using immersed boundary method based solver that has been previously validated for these types of flows [24–26]. To realize our objectives, we compare the ventricular flow patterns and quantify velocity profile differences between the physiological model and a simplified model that includes only LV and Ao, with the LA being modeled as a simple pipe created by extruding the MO along its axis.

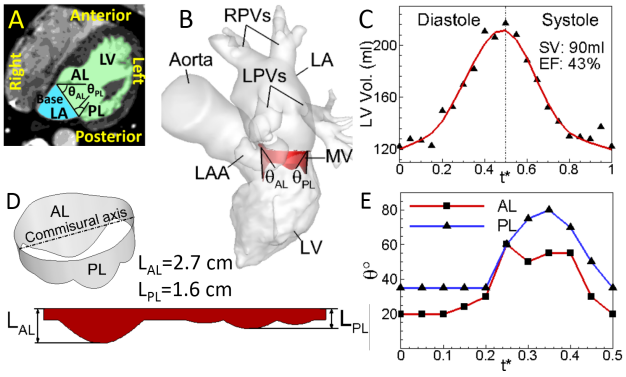

Fig. 1. (A) Axial slice of contrast enhanced CT data with highlighted chambers of left heart. (B) Reconstructed chambers of left heart model from the volume CT data with the indicated nomenclature. (C) Time variation of LV volume (solid) and its time derivative (dotted) during the cardiac cycle. (D) 3D rendering and a flattened cylindrical projection of MV. (E) Measurement of MV leaflet angles with respect to the base or mitral annulus plane as shown in Fig. 1A-B. LPVs/RPVs: left/right pulmonary veins; LA: left atrium; LAA: left atrial appendage; MV: mitral valve; AL: anterior leaflet; PL: posterior leaflet; LAL, LPL: maximum lengths of AL and PL; LV: left ventricle; Ao: Aorta; SV: stroke volume; EF: ejection fraction.

2 Methods

2.1 Geometric Left Heart Model

The heart model is based on a high-resolution 4D CT scan of an adult male (see Fig. 1A). The scanner employed is Toshiba 320 Aquilon-One multi-detector scanner (Toshiba Medical Systems Inc.) with a voxel resolution of about 0.43x0.43x0.5 mm3 (512x512x280 voxels) and a temporal resolution of 0.06s (20 volume frames per cycle). Each of these volume images is subjected to filtering using median filter for noise reduction and thresholding for contrast enhancement [27] until the blood lumen is clearly distinguished from the tissue. Segmentation is then performed using the region growing algorithm [27] in commercial software (Mimics, Materialise Inc). The errors associated with image acquisition, processing and segmentation generate noticeable spurious variation in the volume-time curve (see Fig. 1C) and a smooth spline is therefore fit through these points and then used for temporal interpolation between the key frames as described in the next section (Fig. 1C).

The ejection fraction (EF=43%, see Fig. 1C) of the present model is lower than the value of 55% considered typical for a healthy adult, but the current stroke volume (SV) of 90 ml is found to be within the normal range of 60-100 ml. Furthermore, the heart of the subject in this study was judged by the cardiologist to be functionally normal. Given the absence of any underlying cardiac pathology and the fact

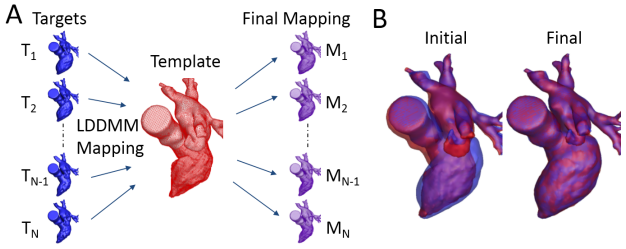

Fig. 2. (A) Schematic of volume registration of each target cardiac phase with respect to the template using large deformation diffeomorphic metric mapping (LDDMM) method. (B) An example mapping of the end-systolic state (template, red) with the end-diastolic state (target, blue) using LDDMM.

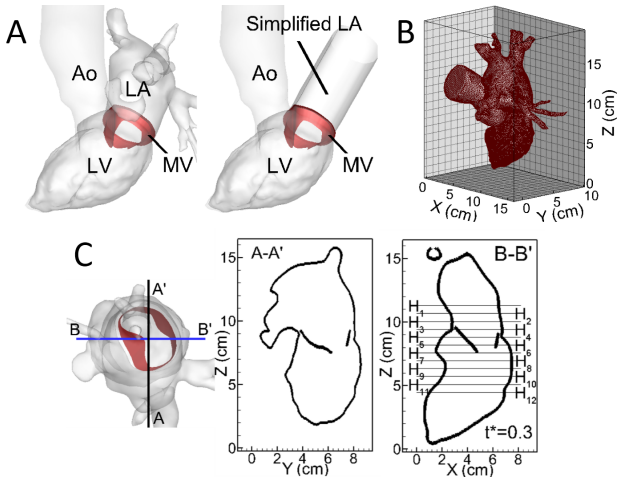

Fig. 3. (A) Computational models used in the present study: (left) physiological left heart model with anatomically correct LA, LV, and Ao; (right) simplified atrium model where the filling into LV takes place from a pipe created by outward extrusion of MO along its axis. Both these models have identical MV configuration as highlighted. (B) Computational domain with the physiological model immersed into it. (C) Orthogonal cross-sectional planes (A-A, B-B) used for analysis of hemodynamic data together with transverse sections on B-B plane to probe velocity profiles. LA: left atrium; LV: left ventricle; MV: mitral valve; Ao: Aorta.

that atrial fluid dynamics is driven primarily by the stroke volume and not the LV ejection-fraction, it is expected that the lower than typical ejection fraction will not affect the primary observations and conclusions of the current study.

The mitral valve (MV) is a bileaflet atrio-ventricular valve that was recently shown to promote looping of the flow from the ventricular lateral wall to the septal wall [22] and also that the vortices formed on its leaflets assist LV filling [28]. Thus, any model attempting to predict ventricular flow patterns should include a sufficiently accurate representation of the MV. The MV morphology is based on earlier *in vivo* measurements [23] (see Fig. 1D) and for the valve leaflet motion, we have employed a prescribed kinematics model [22, 29] in which the angles made by each of the leaflets with respect to the base of the mitral valve (θ_{AL}, θ_{PL}) are measured from the CT data (see Fig. 1E), and this angular deflection is smoothly distributed across the span of the leaflets [22]. Although the present model is simplified in both its geometry and motion, this approach has been shown to be a reasonable physiological representative that captures the key LV flow features [22]. Additionally, the velocity of the material points on the mitral valve leaflets was found to range up to 30 cm/s, which is within the range of physiologically measured values (¡40 cm/s, [30]).

The outcome of image processing of 4D CT data is a set of triangulated surfaces for each of the 20 key frames over the entire cardiac cycle. However, since each key frame is processed independent of the others, the generated triangulated surfaces for the different frames do not maintain a conformal mesh topology across all the key frames; instead, each surface has different number of nodes and connectivity. Therefore, it is necessary to register each of these surfaces to a chosen template and create a smooth mapping across all the key frames (or targets) to be able to prescribe this moving surface as a boundary condition for the flow solver (see Fig. 2). We employ a diffeomorphic registration algorithm known as Large Deformation Diffeomorphic Metric Mapping (LDDMM) [31] that can conveniently support large deformations and further details on its implementation and underlying mathematics are provided in [32]. We have employed a similar registration procedure for the MV model as well because the MV is not fixed at one position; instead changes its configuration considerably during the cardiac cycle [6, 28, 33].

In general, the temporal resolution of the cardiac CT, which is limited to about 20 frames per cardiac cycle, is not sufficient to directly perform numerical simulations of blood flow. Hence, we follow the generic procedure [10, 29, 34] to interpolate the triangulated surfaces in time after performing the LDDMM registration. We employ a periodic cubic spline interpolation of the position coordinates of these surfaces in time, which ensures continuity of both velocity and acceleration while retaining the periodicity of the cardiac cycle. The aorta is modeled as a rigid surface, and is allowed to move as per the dynamic CT imaging.

In order to investigate the effect of atrial flow patterns on the ventricular flow, we have created two different computational models- the first model comprises a physiological left heart model with all the major chambers- LA, LV, and Ao (left frame, Fig. 3A) and in the second model, the LA is replaced by a pipe (right frame, Fig. 3A) via outward extrusion of the MO along its axis. It is to be noted that both these models have the same MV model included as a part of the LV. Hence, we have two models under investigation with near-identical topology and kinematics of LV and MV, with only the atrium being different. A zero gradient velocity boundary condition is provided at all the open boundaries such as the PVs for the physiological model, and at the pipe inflow for the simplified model. The outflow tract is fully closed during diastole and is opened using zero gradient velocity condition at outlet during systole for both these models; similarly, the mitral valve is fully closed during ventricular systole, thereby

preventing any mitral regurgitation.

2.2 Hemodynamics Modeling and Flow Solver

Blood flow in the major chambers of the heart is modeled as Newtonian flow governed by the Navier-Stokes equations for unsteady, incompressible flows,

$$\nabla.\vec{u} = 0$$
$$\rho\left[\frac{\partial\vec{u}}{\partial t} + \vec{u}.\nabla\vec{u}\right] = -\nabla p + \mu\nabla^2\vec{u} \qquad (1)$$

where, $\vec{u}$ is the velocity vector, p is the pressure, and ρ and μ are the density and the viscosity of the blood, respectively. The equations are discretized using a second-order, cell-centered, collocated grid arrangement of the primitive variables, $\vec{u}$ and p on a non-body-conforming Cartesian grid. The motion of the moving bodies is treated using a sharp-interface immersed boundary method based on the multi-dimensional ghost-cell methodology (GCM) described in Mittal et al. [24, 25, 35].

The heart model used here is discretized with 52,852 triangular surface elements while the MV is represented using 12,000 elements. The entire surface is immersed in a Cartesian grid of size 11.5cm x 9.5cm x 15.8cm covered by a total of 384x256x256 (25.2 million) cells (Fig. 3B). The resolution is chosen based on previous computational studies where a thorough grid convergence study [15, 17] and validation [26] has been performed. The flow Reynolds number (Re) based on peak diastolic area-averaged mitral velocity and mitral annulus diameter is about 2420 while the Womersley number (Wo) based on mitral annulus diameter and cardiac cycle duration (1.2 sec) is 19. Simulations are performed on the Stampede high performance computing cluster (located at the Texas Advanced Computing Center) with 512 CPU cores for 3 cardiac cycles and the computation for one cardiac cycle takes about 3 days. The cycle-to-cycle variation of all computed average quantities is less than 5% and therefore, three cycles are considered sufficient for our analysis. Computed phase-averaged data along two orthogonal cross-sectional planes, (A-A) and (B-B) as shown in Fig. 3C, is then used for comparison between the two computational models (physiological and simplified). Figure 3C also highlights the various cross-sections ($H_1 - H_{12}$) along B-B plane used to compare the profiles of longitudinal component of velocity between the physiological and simplified atrium models.

3 Results

3.1 Atrial Flow Patterns and Vortex Topology

In this section, we describe the key features of the atrial flow patterns and vortex topology, especially with the aim of comparing them to previous data and to facilitate a deeper understanding of atrial vortex dynamics. The flows from the LPVs and RPVs exhibit very different behavior throughout

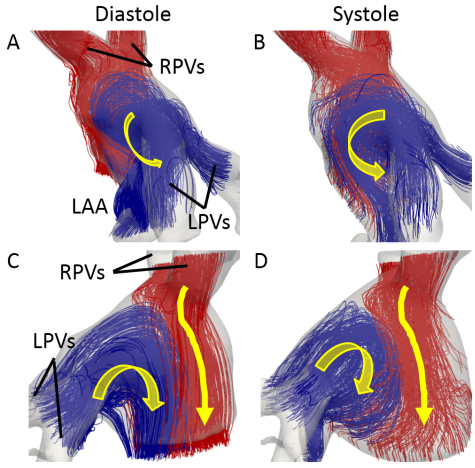

Fig. 4. Streamlines visualization in LA during diastole (A, C) and systole (B, D) in two different views. Streams emanating from the LPVs and RPVs are colored differently (blue and red, respectively) for better visualization and understanding of LA flow patterns. LPVs/RPVs: left/right pulmonary veins; MO: mitral orifice; LAA; left atrial appendage.

the cardiac cycle (Fig. 4). A complex looping of the flow ejected from the LPVs could be clearly identified whereas the flow from the RPVs forms a direct stream towards the mitral annulus confined between LPVs generated circulatory flow and the outer periphery of LA (Fig. 4). While during diastole (Figs. 4A, 4C), the flow from both the veins smoothly enters the mitral orifice when the MV is open; during systole when the MV is closed (Figs. 3B, 4D), the flow from RPVs decelerates and forms an outer loop around the inner circulatory flow due to LPVs. These features were also described in earlier studies [7, 34]. Although not directly shown here, we have also detected flow reversal in the PVs during late atrial systole [34, 36] and a flow ratio of about 3:5 between the LPVs and RPVs throughout the cardiac cycle.

Interesting vortex dynamics are exhibited inside the LA cavity (Fig. 5) which was not well-understood earlier. As the atrial wall expands, four small vortex rings are ejected from the pulmonary veins (Fig. 5A) and these are observed to propagate towards the center of the atrial cavity (Fig. 5B) which is in line with previous experimental measurements [9]. The propagation of these vortex rings brings them into direct interaction (Figs. 4B-D) with each other and this leads to a vortex breakup and dissociation into a number of dissipating small-scale vortex structures (Figs. 4E-F). Collision of vortex rings at various inclination angles and their subsequent breakdown due to the non-uniform stretching and enhanced viscous dissipation has been studied extensively in the past [37] in a simplified experimental setup and it is interesting to observe this phenomenon occur in a realistic setting of LA. The complexity of the present case is further accentuated by the collision of four vortex rings emanating from the PVs. A complex flow due to the interaction of these vortices in the upper part of the LA has also been noted in the earlier simulations [34].

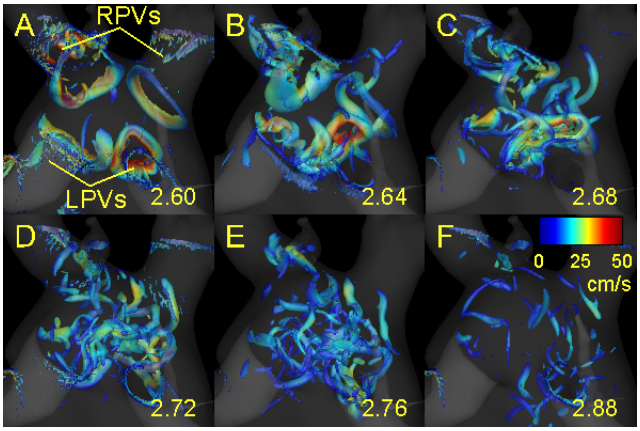

Fig. 5. Left atrial vortex dynamics and breakdown during ventricular systole. Instantaneous vortex structures are visualized using λ_{ci} criterion [38] colored by the magnitude of velocity and the numbers indicate non-dimensional times during the 3^{rd} cardiac cycle.

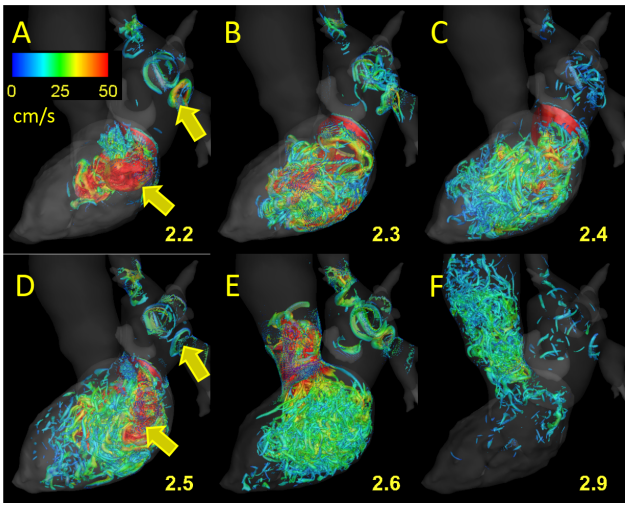

Fig. 6. Vortex structures in the physiological model colored by the magnitude of velocity. Numbers indicate various non-dimensional times during the 3^{rd} cardiac cycle.

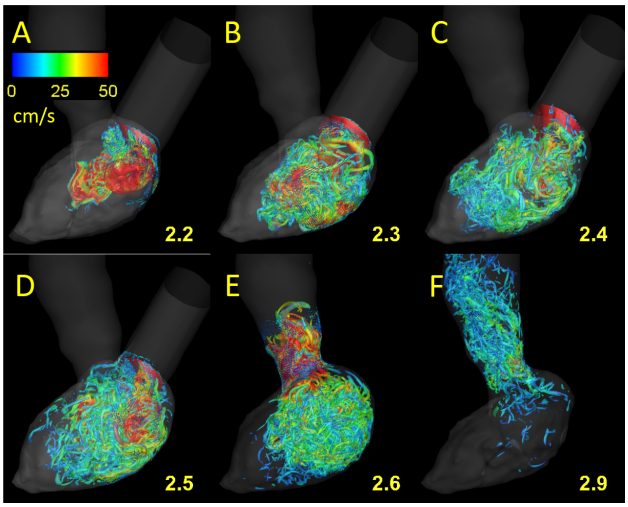

Fig. 7. Same as Fig. 6 but for the simplified model.

Vorticity annihilation between the vortex patches of opposite rotation is another key mechanism for the rapid diminishment of these vortices. The outcome of all these combined effects of collision, annihilation and enhanced viscous dissipation is that the coherent vortex rings generated by the PVs at the beginning of ventricular systole have mostly disappeared by the beginning of ventricular diastole. Thus, as the MV opens during diastole, we expect there to be little interaction in terms of convection of atrial vortices into the ventricle. Further discussion regarding atrio-ventricular vortex structures is presented in the following section.

3.2 Atrio-ventricular Vortex Patterns

Figure 6 shows instantaneous vortex structures during the 3^{rd} cardiac cycle in the physiological model at the indicated time instants. As previously reported [14–16,28,34,39,40], a vortex ring can be identified pinching off from the mitral leaflets during early diastole (Fig. 6A) and it propagates towards the lateral wall. At the same time, the LA, which acts as a passive conduit in this instance, is filled with vortex rings ejected from each of the PVs. Subsequently (Fig. 6B), the diastolic ventricular vortex impinges onto the LV lateral wall and breaks up, giving rise to several small-scale vortex structures. During this same period, the vortices from the pulmonary veins in the LA interact with each other and disintegrate before being scattered in the atrial cavity. As the flow advances into the LV cavity towards the apex due to fluid inertia (Fig. 6C), the atrial vortices are found to rapidly dissipate in the atrial cavity. By the end of diastole (Fig. 6D), the atrial contraction produces distinct vortex rings in LA and also generates another strong vortex ring in the LV. The movement of the vortices from the anterior to the posterior wall suggests an overall clockwise flow pattern in the ventricular cavity, which has been observed by several investigators in the past [8, 11, 15, 22, 41–44].

During ventricular systole (Figs. 6E-F), the flow from the ventricle is ejected out into the aorta through the outflow tract as a highly transitional jet at high velocities. However, by the end of systole, the ventricular cavity is almost devoid of any vortical structures before the onset of the next cardiac cycle. On the other hand, the LA, which acts as a reservoir, is refilled with vortices from the pulmonary veins during ventricular systole. However, these vortices interact and dissipate towards the end of filling (as noted in the previous subsection, Fig. 5) following which, a fresh cycle is repeated.

Figure 7 shows vortex structures in the ventricle of the second model with a pipe replacing the atrium, at time-instants identical to that of Fig. 6. Qualitatively, no major differences could be identified between the ventricular vortex structures in the two models despite the development of a complex three-dimensional vortical field in the LA of the physiological model.

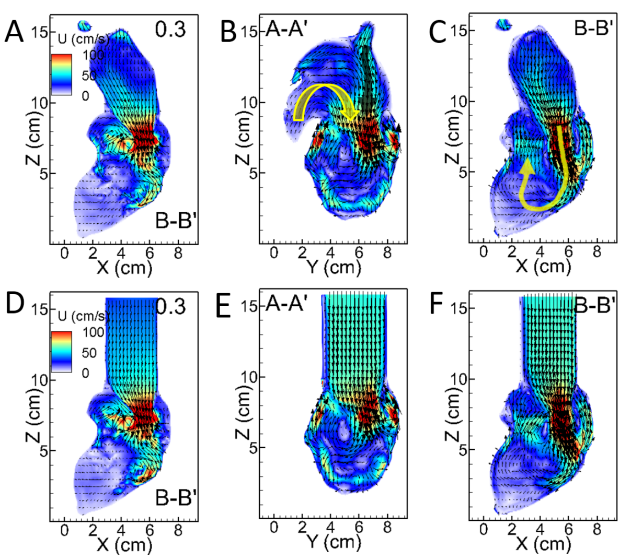

Fig. 8. Comparison of averaged flow field between physiological (top) and simplified (bottom) models. (A, D) Phase-averaged velocity fields along B-B plane during mid-diastole. (C-D, E-F) Phase-time-averaged velocity field during entire diastole along the indicated reference planes (A-A and B-B). See Fig. 3C for plane configuration.

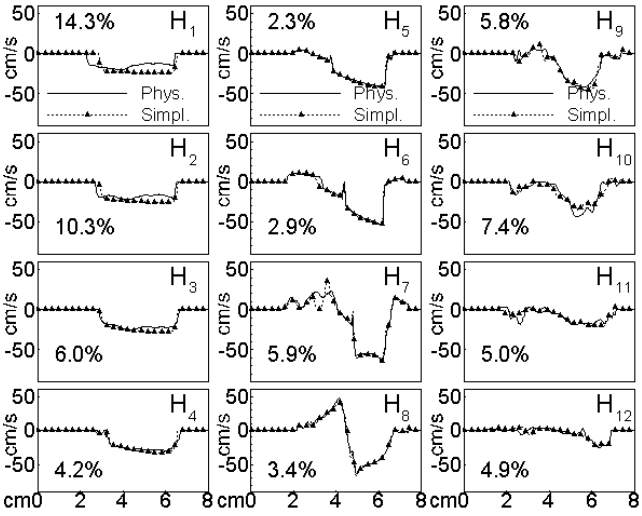

Fig. 9. Comparison of longitudinal velocity component profiles at various transverse sections (H_1-H_{12}) of B-B plane during mid-diastole as shown in Fig. 3C. The L_1 norm of the difference in each profile is quantified as a percentage of peak mitral flow velocity (U_p=63cm/s).

3.3 Averaged Flow

Figure 8 compares the intraventricular velocity field between the physiological model (Figs. 8A-C) and simplified model (Figs. 8D-F). In agreement with the qualitative comparison of vortex structures (Figs. 6, 7), no significant differences could be discerned from the velocity field comparison between the two models in the ventricular cavity not only at distinct time instants (Figs. 8A, 8D) but also with respect to the time-averaged flow during diastole (Fig. 8B-C, 8E-F). Further, it is seen that the velocity vectors in the LA align themselves along the mitral axis and converge smoothly towards the MV (Figs. 8A-C) and this effect is explored further in later sections.

As noted earlier, two distinct flow regimes can be identified in the LA (Fig. 8B): a relatively lower velocity flow that smoothly loops from the LAA towards the MO and fills up most of the LA cavity; and the flow from the RPVs that enters the MO at a relatively higher velocity. Both these streams merge as they approach and accelerate through the MO. In contrast, the flow pattern in the pipe in Fig. 8E is in line with that of a pulsatile flow in a pipe; yet, the flow pattern near MO is quite similar to that observed for the physiological LA model (Fig. 8A, B). This is attributed to the rapid increase in the flow velocity as LA narrows and streamlines the flow before entering MO with a fairly uniform velocity.

3.4 Velocity Profiles

In this section, we provide a more quantitative comparison of the hemodynamic data between the two models by computing the L_1 norm of the difference in longitudinal component of velocity between the two models along various transverse sections (see Fig. 9). The plots indicate notable differences in the flow velocity profiles inside the LA cavity and the region proximal to the MO. Among all the velocity profiles, H_1 records the highest deviation (14.3%) of physiological model with respect to the simplified model. This is attributed to the larger cross-sectional area of the physiological atrium at the level of H_1 than that of the simplified model where the cross-sectional area is same as that of the mitral annular area. Hence, a diffused velocity profile is found in the LA of the physiological model. However, as the flow is guided into a reduced cross-section at H_2 and H_3, the flow gets streamlined and hence, catches up with that of the simplified model substantiated by the gradual reduction in the L_1 norm of the difference from 10.3% (H_2) to 4.2% (H_4). Eventually, both the profiles become almost indistinguishable at the mitral orifice (H_4) with a near-uniform velocity profile.

The difference in the velocity profiles decreases further as the flow is guided through the MO by the valve leaflets at H_5 and H_6 with each profile contributing to a normalized difference of less than 3%. The asymmetric alignment of the mitral leaflets, causing the anterior leaflet to have a lesser opening than the posterior leaflet, skews the jet towards the lateral wall (H_5-H_7). After impingement, regions of reversed flow could be seen originating near the tips of the mitral leaflets (H_7) due to vortex ring and the mildly sharper peaks begin to diffuse across the section down into the ventricular cavity (H_8-H_9).

Subsequently, the flow decelerates and produces a diffused velocity profile that spreads towards the septal wall (H_{10}-H_{12}). Although the velocity profiles nearly overlap at the level of the mitral orifice (H_3-H_5), the same is not strictly reflected in the ventricular cavity which could be due to small local differences in the geometry and motion of the ventricle and the valves between the two models as a result of diffeomorphic mapping. Additionally, small perturbations intro-

duced in the LA could gradually amplify and manifest themselves in the ventricular cavity due to the highly transitional nature of the flow. Nevertheless, the profiles exhibit a maximum difference of about 7% in the ventricular cavity despite the complex LA anatomy and the associated flow field. It is also noted that the maximum L_1 norm of the point-wise difference of each component of the velocity in the ventricle is only 10% of the peak mitral flow velocity (U_p).

4 Discussion

In the present study, numerical simulations have been used to understand the role of the atrial vortices and flow patterns on the development of diastolic ventricular flow patterns. Two distinct models are employed in this study: in the first model, medical imaging data is used to create a multi-chamber model of the left heart that includes LA, LV and Ao; whereas in the latter, the LA is simplified while the other chambers (LV and Ao) are retained. The simplification of LA involves outward extrusion of the mitral orifice along its axis to form a pipe through which the filling takes place into LV. As it is already proven that MV has a significant role on ventricular fluid dynamics [22, 28], we include identical MV models in both these heart models. The MV models employed here are based on prescribed kinematics [22] using physiological data, which although not strictly subject-specific, is still expected to be a sufficiently reasonable representative of the physiological MV.

The LV is arguably the most important chamber of the mammalian heart since it provides much of the pumping power that drives blood to the body and is also the component of the heart that is most susceptible to cardivascular disease. Consequently a vast number of experimental and computational modeling studies of the heart have focused on modeling LV hemodynamics [11–19, 21, 22, 34, 41, 45, 46]. In most of these models, it has been customary to model the LA as a simple pipe attached to the LV at the MO. Recent advances in medical imaging have expanded the scope of modeling intraventricular flows from simple canonical shapes to complex image-based flow modeling strategies and thus, provide an opportunity to explore atrio-ventricular hemodynamic interaction [10, 34]. Therefore, the study design that is employed here is well suited to understand the coupling between atrial and ventricular hemodynamics.

The simulations presented here were conducted on a high resolution Cartesian grid comprising about 25.2 million cells. Computed flow field has been visualized here using streamlines (Fig. 4), three dimensional vortex structures (Figs. 5-7) and averaged velocity field along cross-sectional planes (Fig. 8). It is noted that the ventricular flow field obtained here correlates well with previous studies. Firstly, a uniform plug flow profile is seen near the mitral orifice which has been described in the past [43, 44]. Secondly, a vortex ring is seen to be pinched off from the tips of mitral leaflets which propagates and impinges on the lateral wall. This has also been well established in the past [8, 10, 34, 40, 44, 47]. Subsequently, the vortex ring disintegrates and a circulatory flow pattern is produced in the ventricular cavity that sweeps the flow from the lateral wall along the apical region towards the septum [8, 10, 15, 22, 28, 40, 42, 48, 49].

It is noted that the present simulations not only predict the ventricular flow that is consistent with the previous works but also predict the flow inside LA that is generally in line with clinical measurements. For instance, velocity measurements in the LA using 3D phase contrast MRI [7] indicated that the flow from superior RPV is confined between the LA cavity flow and the atrial wall while the flow from the LAA and the nearby LPV loops to enter the mitral orifice. These flow features are reproduced in the current study as well.

Vortex rings in the left atrium are primarily produced from the pulmonary veins in the upper part of the atrial cavity and these structures undergo mutual interaction leading to a complex flow field (Fig. 4-5). The development of four vortex rings from each of the pulmonary veins at an angle to each other, circumscribed by a moving wall, leads to non-uniform stretching and breakup of these vortex rings producing a highly complex flow in the upper part of the LA [34]. This, coupled with vorticity annihilation and viscous dissipation, leads to a rapid decay of these vortices by the onset of diastole. The interacting vortex rings are also expected to enhance mixing inside the LA [7] which suggests that the unique morphology of the LA enhances mixing and avoids stasis in the atrium [7]. However, while the flow inside LA seems to promote mixing and washout, the rapid dissipation of the vortices leads to a highly regularized, nearly uniform flow through the mitral annulus.

The simulations indicate that the complex flow features in the atrium have an insignificant impact on the ventricular filling. 3D vortex structures (Figs. 6-7) and averaged velocity fields (Fig. 8) in the LV do not show any noticeable differences between the simplified and the physiological atrium models. Velocity profiles plotted along B-B plane (Fig. 9) and global velocity differences in terms of the L_1 norm indicate that the maximum difference in the velocities between the two models is about 10% of U_p. This is in contrast to the observations of Mihalef et al. [10] who indicated that vorticity is introduced in the PVs and transported through the mitral orifice into the LV cavity. They further surmised that not accounting for this vorticity transport would produce similar LV flow patterns with or without the presence of LA. However, in the present study, we demonstrate, using a study design that is more suited to understand the effect of LA flow patterns on LV hemodynamics, that such a transport model is not necessary. This is because most of the vorticity that is introduced in the LA is dissipated and does not survive the passage through the MO.

The above observations have important clinical implications; they indicate that the morphology and physiology of the LA is designed so as to promote mixing and washout but at the same time, generate a highly regularized flow at the mitral annulus. From the point-of-view of cardiac physiology, this implies that small changes in the LA dynamics would not cascade into the functioning of LV which is, arguably, the most critical element of the cardiac pump. This suggests a certain level of inherent robustness in the functioning of the left heart. Interestingly, significant variations

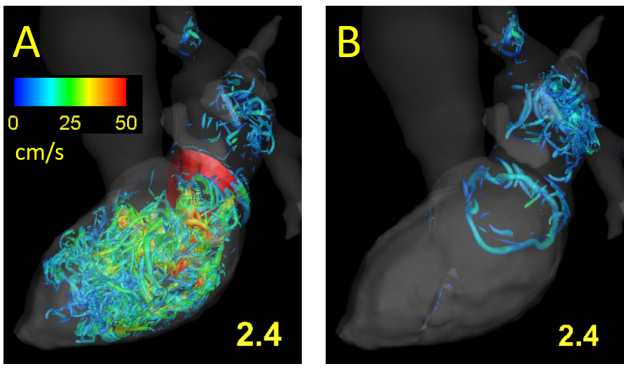

Fig. 10. Comparison of vortex structures during late diastole of the 3^{rd} cycle (t*=2.4) between the physiological model with MV (A) and without MV (B).

in the number of pulmonary vein ostia have been detected in the general population [50], and the current study suggests that such variations would not directly impact the LV hemodynamics. Additionally, the study also suggests that certain surgical procedures involving the LA such as LAA closure or LAA occlusion performed on patients with atrial fibrillation and LAA clots, likely will not induce significant alterations in LV hemodynamics as long as the functional features such as the atrial stroke volume and the timing of atrial contractions are unaffected. The robustness of the LV flow might, however, be affected by the presence of other significant ventricular or valvular pathologies in ways that are not predicted by the current study.

The second implication of the above observations is that simple models of LA should suffice in computational or experimental studies where the phenomenon of interest is related to the ventricle or anything downstream of it. In our own study for instance, we have found that the use of the simple pipe-shaped LA reduces computational cost by over 25% compared to the physiological LA. For experimental models, this also implies that significant simplification could be made in the modeling of the LA.

A recent study [22] has examined the effect of MV on ventricular flow patterns using a pipe-based LA model. By comparing the flow patterns between a model that includes MV and the one that does not, the study found that the valve produces significant changes not only in the filling velocity but also in the overall rotational motion, mixing and washout associated with the mitral jet. Coupled with the results of the current study, it may be concluded that the MV model is far more essential for accurate modeling of the ventricular flow than a physiological LA model.

In order to confirm this, we have considered a case where the MV is removed from the physiological model and simulations have been conducted for the blood flow in this no-valve model in exactly the same way as was performed previously for the with-MV model and the results compared in Fig. 10. Clearly, significant differences in the ventricular vortex topology could be discerned after MV removal. The vortex ring is positioned closer to the MO throughout the cardiac cycle for the no-valve model and exhibits reduced penetration into the LV cavity similar to that observed in the past studies [14, 51]. This is because the flow is not constrained between the narrowing cross-section formed by the asymmetric leaflets and hence, does not accelerate to higher velocities sweeping the flow from the lateral wall to the septum.

We note finally that although the present model is based on 4D CT data that has direct clinical relevance and patient-specific attributes, the mitral-valve employed here is not patient-specific and does not account for fluid-structure-interaction. The kinematic valve model has, however, been shown to be a reasonable physiological representative that captures the key LV flow features [22]. Secondly, the LV model does not include surface trabeculae or papillary muscles on the ventricular endocardium since this significantly increased the preprocessing and simulation effort. However, while the trabeculae and papillary muscles do affect the LV flow [52], this is not expected to significantly affect the key conclusion of the current study due to the use of a comparative study design that employs the same LV model for all the cases.

5 Conclusions

Numerical simulations have been used to elucidate the flow and vortex patterns in the left atrium and their effects on the dynamics of ventricular flows. The vortex topology in the left atrium is dominated by the generation and interaction of vortex rings from the four pulmonary veins. However, the vortex breakup and annihilation are observed to rapidly diminish the strength of these vortices. The flow pattern in the left atrium is characterized by a circulatory flow generated by the left pulmonary veins and a direct stream from the right-pulmonary veins to the mitral annulus. These patterns are in general agreement with previous studies [7, 9].

Due to the rapid dissipation of the vortices in the atrium, the flow through the mitral valve during ventricular diastole is highly regularized and a comparison of the physiological and pipe models of the left atrium shows that the overall differences in the ventricular flow velocity between the two models is limited to about 10% of the peak mitral flow velocity. This suggests that the morphology and physiology of the left atrium is designed so as to enhance the robustness of the hemodynamics of the left ventricle to the dynamics of the left atrium, and this has clinical implications for pathologies, as well as surgical therapies involving the left atrium. This also implies that significant simplifications can be made in computational and experimental models that are focused on investigating ventricular hemodynamics.

Acknowledgements

This research is supported by NSF through grants IOS-1124804, IIS-1344772 and TG-CTS100002 and by the Johns Hopkins Medicine Discovery Award. R.T.G. reports research support from Astellas Pharma, General Electric, Toshiba Medical Systems Corporation and Caprior, Inc. R.T.G. is a consultant for the ICON Medical Imaging.

References

[1] Al-Saady, N. M., Obel, O. A., and Camm, A. J., 1999. "Left atrial appendage: structure, function, and role in thromboembolism". *Heart,* **82**(5), pp. 547–554.

[2] Stefanadis, C., Dernellis, J., and Toutouzas, P., 2001. "A clinical appraisal of left atrial function". *Eur. Heart J.,* **22**(1), pp. 22–36.

[3] Ho, S. Y., Cabrera, J. A., and Sánchez-Quintana, D., 2012. "Left atrial anatomy revisited". *Circ: Arrhythm Electrophysiol.,* **5**(1), pp. 220–228.

[4] Agmon, Y., Khandheria, B. K., Gentile, F., and Seward, J. B., 1999. "Echocardiographic assessment of the left atrial appendage". *J. Am. Coll. Cardiol.,,* **34**(7), pp. 1867–1877.

[5] Koizumi, R., Funamoto, K., Hayase, T., Kanke, Y., Shibata, M., Shiraishi, Y., and Yambe, T., 2015. "Numerical analysis of hemodynamic changes in the left atrium due to atrial fibrillation". *J. Biomech.,* **48**(3), pp. 472–478.

[6] Appleton, C. P., and Kovács, S. J., 2009. "The role of left atrial function in diastolic heart failure". *Circ: Cardiovasc Imaging,* **2**(1), pp. 6–9.

[7] Fyrenius, A., Wigström, L., Ebbers, T., Karlsson, M., Engvall, J., and Bolger, A. F., 2001. "Three dimensional flow in the human left atrium". *Heart,* **86**(4), pp. 448–455.

[8] Kilner, P. J., Yang, G. Z., Wilkes, A. J., Mohiaddin, R. H., Firmin, D. N., and Yacoub, M. H., 2000. "Asymmetric redirection of flow through the heart". *Nature,* **404**, pp. 759–761.

[9] Park, K.-H., Son, J.-W., Park, W.-J., Lee, S.-H., Kim, U., Park, J.-S., Shin, D.-G., Kim, Y.-J., Choi, J.-H., Houle, H., et al., 2013. "Characterization of the left atrial vortex flow by two-dimensional transesophageal contrast echocardiography using particle image velocimetry". *Ultrasound Med. Biol.,* **39**(1), pp. 62–71.

[10] Mihalef, V., Ionasec, R. I., Sharma, P., Georgescu, B., Voigt, I., Suehling, M., and Comaniciu, D., 2011. "Patient-specific modeling of whole heart anatomy, dynamics and haemodynamics from four-dimensional cardiac CT images". *J. Roy. Soc. Int. Focus,* **1**, pp. 286–296.

[11] Domenichini, F., Pedrizzetti, G., and Baccani, B., 2005. "Three-dimensional filling flow into a model left ventricle". *J. Fluid Mech.,* **539**, pp. 179–198.

[12] Schenkel, T., Malve, M., Reik, M., Markl, M., Jung, B., and Oertel, H., 2009. "MRI-based CFD analysis of flow in a human left ventricle: methodology and application to a healthy heart". *Ann. Biomed. Eng.,* **37**(3), pp. 503–515.

[13] Krittian, S., Schenkel, T., Janoske, U., and Oertel, H., 2010. "Partitioned fluid-solid coupling for cardiovascular blood flow: validation study of pressure-driven fluid-domain deformation". *Ann. Biomed. Eng.,* **38**(8), pp. 2676–2689.

[14] Le, T. B., and Sotiropoulos, F., 2012. "On the three-dimensional vortical structure of early diastolic flow in a patient-specific left ventricle". *Eur. J. Mech. B-Fluids,* **35**, pp. 20–24.

[15] Seo, J. H., and Mittal, R., 2013. "Effect of diastolic flow patterns on the function of the left ventricle". *Phys. Fluids,* **25**(11), pp. 110801:1–21.

[16] Doenst, T., Spiegel, K., Reik, M., Markl, M., Hennig, J., Nitzsche, S., Beyersdorf, F., and Oertel, H., 2009. "Fluid-dynamic modeling of the human left ventricle: methodology and application to surgical ventricular reconstruction". *Annals Throac. Surg.,* **87**(11), pp. 1187–1195.

[17] Zheng, X., Seo, J. H., Vedula, V., Abraham, T., and Mittal, R., 2012. "Computational modeling and analysis of intracardiac flows in simple models of left ventricle". *Eur. J. Mech. B-Fluids,* **35**, pp. 31–39.

[18] Seo, J. H., Vedula, V., Abraham, T., and Mittal, R., 2013. "Multiphysics computational models for cardiac flow and virtual cardiography". *Int. J. Numer. Meth. Biomed. Eng.,* **29**(8), pp. 850–869.

[19] Saber, N. R., Wood, N. B., Gosman, A. D., Merrifield, R. D., Yang, G. Z., Charrier, C. L., Gatehouse, P. D., and Firmin, D. N., 2003. "Progress towards patient-specific computational flow modeling of the left heart via combination of magnetic resonance imaging with computational fluid dynamics". *Ann. Biomed. Eng.,* **31**, pp. 42–52.

[20] Pasipoularides, A. D., Shu, M., Womack, M. S., Shah, A., Ramm, O. V., and Glower, D. D., 2003. "Rv functional imaging: 3-d echo-derived dynamic geometry and flow field simulations". *Am. J. Physiol.- Heart Circ. Physiol.,* **284**, pp. H56–65.

[21] Long, Q., Merrifield, R., Yang, G., Xu, X., Kilner, P., and Firmin, D., 2003. "The influence of inflow boundary conditions on intra left ventricle flow predictions". *J. Biomech. Eng.,* **125**(6), pp. 922–927.

[22] Seo, J. H., Vedula, V., Abraham, T., Lardo, A., Dawoud, F., Luo, H., and Mittal, R., 2014. "Effect of the mitral valve on diastolic flow patterns". *Phys. Fluids,* **26**(12), pp. 121901:1–14.

[23] Ranganathan, N., Lam, J., Wigle, E., and Silver, M., 1970. "Morphology of the human mitral valve ii. the valve leaflets". *Circulation,* **41**(3), pp. 459–467.

[24] Mittal, R., Dong, H., Bozkurttas, M., Najjar, F. M., Vargas, A., and von Loebbecke, A., 2008. "A versatile sharp interface immersed boundary method for incompressible flows with complex boundaries". *J. Comput. Phys.,* **227**, pp. 4825–4852.

[25] Seo, J. H., and Mittal, R., 2011. "A sharp-interface immersed boundary method with improved mass conservation and reduced spurious pressure oscillations". *J. Comput. Phys.,* **230**, pp. 7347–7363.

[26] Vedula, V., Fortini, S., Seo, J. H., Querzoli, G., and Mittal, R., 2014. "Computational modeling and validation of intraventricular flow in a simple model of the left ventricle". *Theor. and Comp. Fluid Dyn.,* **28**(6), pp. 589–604.

[27] Rangayyan, R. M., 2004. *Biomedical image analysis*. CRC press-Taylor & Francis group.

[28] Charonko, J. J., Kumar, R., Stewart, K., Little, W. C., and Vlachos, P. P., 2013. "Vortices formed on mitral valve tips aid normal left ventricular filling". *Ann. of Biomed. Eng.,* **41**(5), pp. 1049–1061.

[29] Kulp, S., Gao, M., Zhang, S., Qian, Z., Voros, S., Metaxas, D., and Axel, L., 2011. "Using high resolution cardiac ct data to model and visualize patient-specific interactions between trabeculae and blood flow". In *Medical Image Computing and Computer-Assisted Intervention–MICCAI 2011*. Springer, pp. 468–475.

[30] Upton, M. T., Gibson, D. G., and Brown, D. J., 1976. "Instantaneous mitral valve leaflet velocity and its relation to left ventricular wall movement in normal subjects". *Br. Heart J.,* **38**(1), pp. 51–58.

[31] Beg, M. F., Miller, M. I., Trouvé, A., and Younes, L., 2005. "Computing large deformation metric mappings via geodesic flows of diffeomorphisms". *Int. J. Comput. Vision,* **61**(2), pp. 139–157.

[32] Ardekani, S., Jain, A., Jain, S., Abraham, T., Abraham, M., Zimmerman, S., Winslow, R., Miller, M., and Younes, L., 2012. "Matching sparse sets of cardiac image cross-sections using large deformation diffeomorphic metric mapping algorithm". In *Statistical Atlases and Computational Models of the Heart. Imaging and Modelling Challenges*, O. Camara, E. Konukoglu, M. Pop, K. Rhode, M. Sermesant, and A. Young, eds., Vol. 7085 of *Lecture Notes in Computer Science*. Springer Berlin Heidelberg, pp. 234–243.

[33] Timek, T. A., and Miller, D. C., 2001. "Experimental and clinical assessment of mitral annular area and dynamics: what are we actually measuring?". *Ann. Thorac. Surg.,* **72**(3), pp. 966–974.

[34] Chnafa, C., Mendez, S., and Nicoud, F., 2014. "Image-based large-eddy simulation in a realistic left heart". *Comput. Fluids,* **94**, pp. 173–187.

[35] Mittal, R., and Iaccarino, G., 2005. "Immersed boundary methods". *Ann. Rev. Fluid Mech.,* **37**, pp. 239–261.

[36] Bowman, A. W., and Kovacs, S. J., 2005. "Prediction and assessment of the time-varying effective pulmonary vein area via cardiac mri and doppler echocardiography". *Am. J. Physiol.- Heart Circ. Physiol.,* **288**(5), pp. H280–286.

[37] Lim, T. T., 1989. "An experimental study of a vortex ring interacting with an inclined wall". *Exp. Fluids,* **7**(7), pp. 453–463.

[38] Zhou, J., Adrian, R., Balachandar, S., and Kendall, T., 1999. "Mechanisms for generating coherent packets of hairpin vortices in channel flow". *J. Fluid Mech.,* **387**, pp. 353–396.

[39] Bellhouse, B. J., 1972. "Fluid mechanics of a mitral valve and left ventricle". *Cardiovas. Res.,* **6**, pp. 199–210.

[40] Töger, J., Kanski, M., Carlsson, M., Kovács, S. J., Söderlind, G., Arheden, H., and Heiberg, E., 2012. "Vortex ring formation in the left ventricle of the heart: analysis by 4D flow MRI and Lagrangian coherent structures". *Ann. Biomed. Eng.,* **40**, pp. 2652–2662.

[41] Pedrizzetti, G., and Domenichini, F., 2005. "Nature optimizes swirling flow in the human left ventricle". *Phys. Rev. Lett.,* **95**, pp. 108101:1–4.

[42] Watanabe, H., Sugiura, S., and Hisada, T., 2008. "The looped heart does not save energy by maintaining the momentum of blood flowing in the ventricle". *Am. J. Physiol. Heart Circ. Physiol.,* **294**, pp. H2191–H2196.

[43] Kheradvar, A., Houle, H., Pedrizzetti, G., Tonti, G., Belcik, T., Ashraf, M., Lindner, J. R., Gharib, M., and Sahn, D., 2010. "Echocardiographic particle image velocimetry: a novel technique for quantification of left ventricular blood vorticity pattern". *J. Am. Soc. Echocardiogr.,* **23**(1), pp. 86–94.

[44] Sengupta, P. P., Pedrizzetti, G., Kilner, P. J., Kheradvar, A., Ebbers, T., Tonti, G., Fraser, A. G., and Narula, J., 2012. "Emerging trends in CV flow visualization". *JACC Cardiovasc. Imaging,* **5**(3), pp. 305–316.

[45] Mangual, J. O., Kraigher-Krainer, E., De Luca, A., Toncelli, L., Shah, A., Solomon, S., Galanti, G., Domenichini, F., and Pedrizzetti, G., 2013. "Comparative numerical study on left ventricular fluid dynamics after dilated cardiomyopathy". *J. Biomech.,* **46**(10), pp. 1611–1617.

[46] Choi, Y. J., Vedula, V., and Mittal, R., 2014. "Computational study of the dynamics of a bileaflet mechanical heart valve in the mitral position". *Ann. of Biomed. Eng.,* **42**(8), pp. 1–13.

[47] Pasipoularides, A., 2010. *The heart's vortex: intracardiac blood flow*. PMPH-USA.

[48] Faludi, R., Szulik, M., D'hooge, J., Herijgers, P., Rademakers, F., Pedrizzetti, G., and Voigt, J.-U., 2010. "Left ventricular flow patterns in healthy subjects and patients with prosthetic mitral valves: an in vivo study using echocardiographic particle image velocimetry". *J. Thorac. Cardiovasc. Surg.,* **139**(6), pp. 1501–1510.

[49] Hong, G.-R., Pedrizzetti, G., Tonti, G., Li, P., Wei, Z., Kim, J. K., Baweja, A., Liu, S., Chung, N., Houle, H., et al., 2008. "Characterization and quantification of vortex flow in the human left ventricle by contrast echocardiography using vector particle image velocimetry". *JACC Cardiovasc. Imaging,* **1**(6), pp. 705–717.

[50] Thorning, C., Hamady, M., Liaw, J. V. P., Juli, C., Lim, P. B., Dhawan, R., Peters, N. S., Davies, D. W., Kanagaratnam, P., O'Neill, M. D., et al., 2011. "Ct evaluation of pulmonary venous anatomy variation in patients undergoing catheter ablation for atrial fibrillation". *Clinical imaging,* **35**(1), pp. 1–9.

[51] Le, T. B., Sotiropoulos, F., Coffey, D., and Keefe, D., 2012. "Vortex formation and instability in the left ventricle". *Phys. Fluids,* **24**(9), pp. 091110:1–2.

[52] Vedula, V., Seo, J. H., Lardo, A. C., and Mittal, R., 2014. "Effect of trabeculae and papillary muscles on the hemodynamics of the left ventricle". *Theor. and Comp. Fluid Dyn.*, pp. 1–19.